Understanding the mechanism of the broad-spectrum antiviral favipiravir (T-705): key role of the F1 motif of the viral polymerase

Running title: Exploring the broad-spectrum antiviral effect of T-705

Rana Abdelnabi[1], Ana Theresa Silveira de Morais[2], Pieter Leyssen[1], Isabelle Imbert[2], Stéphanie Beaucourt[3], Hervé Blanc[3], Mathy Froeyen[4], Marco Vignuzzi[3], Bruno Canard[2], Johan Neyts[1#], Leen Delang[1#]*

[1]KU Leuven – University of Leuven, Department of Microbiology and Immunology, Rega Institute for Medical Research, Laboratory of Virology and Chemotherapy, 3000 Leuven, Belgium.

[2]Architecture et Fonction des Macromolécules Biologiques, Centre National de la Recherche Scientifique, Unité Mixte de Recherche 7257, Aix-Marseille Université, 13288 Marseille, France.

[3]Institut Pasteur, Centre National de la Recherche Scientifique UMR 3569, 75724 Paris Cedex 15, France.

[4]KU Leuven – University of Leuven, Department of Pharmaceutical and Pharmacological Sciences, Rega Institute for Medical Research, Laboratory of Medicinal Chemistry, 3000 Leuven, Belgium.

#Equal contribution

***Corresponding author:** Prof. Johan Neyts, Herestraat 49, 3000 Leuven, Belgium. Tel +3216337353, email: Johan.Neyts@kuleuven.be.

Abstract word count: 250

Importance word count: 118

Text word count: 5287

ABSTRACT

Favipiravir (T-705) is a broad-spectrum antiviral agent that has been approved in Japan for treatment of influenza virus infections. T-705 also inhibits the replication of various RNA viruses including chikungunya virus (CHIKV). We demonstrated earlier that the K291R mutation in the F1 motif of the RNA-dependent RNA polymerase (RdRp) of CHIKV is responsible for low-level resistance to T-705. Interestingly, this lysine is highly conserved in the RdRp of positive-sense single-stranded RNA [+ssRNA] viruses. To obtain insights into the unique broad-spectrum antiviral activity of T-705, we explored the role of this lysine using another +ssRNA virus, namely Coxsackievirus B3 (CVB3). Introduction of the corresponding K-to-R substitution in the CVB3 RdRp (K159R) resulted in a non-viable virus. Replication competence of the K159R variant was restored by spontaneous acquisition of an A239G substitution in the RdRp. A mutagenesis analysis at position K159 identified K159M as the only other viable variant, which had also acquired the A239G substitution. The K159 substitutions markedly decreased the processivity of the purified viral RdRp, which was restored by introduction of the A239G mutation. The K159R-A239G and K159M-A239G variants proved, surprisingly, more susceptible to T-705 than the wild-type virus and exhibited lower fidelity in polymerase assays. Furthermore, the K159R-A239G variant was found to be highly attenuated in mice. We thus demonstrate that the conserved lysine in the F1 motif of the RdRp of +ssRNA viruses is involved in the broad-spectrum antiviral activity of T-705 and that it is a key amino acid for the proper functioning of the enzyme.

Key words

Favipiravir; fidelity; mutagenesis; RdRp; CVB3.

IMPORTANCE

In this study, we report the key role of a highly conserved lysine residue of the viral polymerase in the broad-spectrum antiviral activity of favipiravir (T-705) against positive single-stranded RNA viruses. Substitutions of this conserved lysine have a major negative impact on the functionality of the RdRp. Furthermore we show that this lysine is involved in the fidelity of the RdRp and that the RdRp fidelity influences the sensitivity of the virus for the antiviral efficacy of T-705. Consequently, these results provide insights into the mechanism of the antiviral activity of T-705 and may lay the basis for the design of novel chemical scaffolds that may be endowed with a more potent broad-spectrum antiviral activity than T-705.

INTRODUCTION

Favipiravir (T-705) is a broad-spectrum antiviral agent that has been approved in Japan for the treatment of influenza virus infections (1). T-705 has also been reported to inhibit, *in vitro* and in animal models, the replication of different RNA viruses, including norovirus (2), flaviviruses (3) and hantaviruses (4). The compound also showed a potential beneficial effect in the treatment of Ebola virus infected patients in Western Africa during the 2014/2015 outbreak (5).

In the cell, T-705 behaves as a purine analogue and is converted into its ribofuranosyl 5'-triphosphate metabolite (T-705-RTP), after which it can be incorporated in the growing RNA strand as has been shown with the influenza virus RNA-dependent RNA polymerase (RdRp) (1). However, the precise molecular mechanism behind its broad-spectrum antiviral activity has yet to be fully elucidated. Some studies suggest that T-705 inhibits viral RNA synthesis by chain termination of the nascent viral RNA strand (6), while other reports support the induction of lethal mutagenesis (7, 8).

In a previous study from our laboratory, T-705 and its defluorinated analog, T-1105 were shown to inhibit the *in vitro* replication of chikungunya virus (CHIKV) (9). Treatment of CHIKV-infected AG129 mice with T-705 protected these from severe neurological disease and reduced the mortality rate (9). Low-level T-705-resistant CHIKV variants were selected *in vitro* and were shown to have acquired the K291R mutation in motif F1 of the RdRp and a reverse-engineering study corroborated the link between mutant genotype and compound-resistant phenotype (9). Motif F of the RdRp of single-stranded, positive-sense (+ss) RNA viruses has been reported to play an important role in NTP binding during viral RNA synthesis (10). It was also demonstrated that motif F1 of dengue virus is involved in promoter-dependent initiation of RNA synthesis (11). In addition, some residues of motif F of Japanese encephalitis virus were shown to be in-

86 volved in GTP recognition (12). Interestingly, the lysine residue of motif F1 which was
87 mutated in the T-705-resistant CHIKV variants, is highly conserved amongst +ssRNA
88 viruses, a group to which many neglected and emerging viruses belong (**Figure 1**). The
89 exact role of this lysine in viral RdRp activity remains unclear. Given the need for broad-
90 spectrum antivirals, it is thus of great importance to understand how T-705 precisely
91 interacts with the RdRp of RNA viruses. Such information may potentially provide in-
92 sight into how more potent broad-spectrum +ssRNA virus inhibitors can be developed.
93 We here explored whether the conserved lysine in the F1 motif of the viral RdRp is in-
94 volved in the broad-spectrum antiviral activity of T-705. To this end, we used the Cox-
95 sackievirus B3 (CVB3), another +ssRNA virus that is sensitive to T-705 and for which we
96 have the necessary reverse-genetics tools and enzymatic assays available, as the model
97 virus in this study. Using CVB3, we demonstrate for the first time that this highly con-
98 served lysine residue plays a key role in RdRp functionality and fidelity and that a vari-
99 ant of this residue exhibits a highly attenuated phenotype in mice. We next succeeded to
100 elucidate the mechanism of resistance against T-705, thereby demonstrating the role of
101 RdRp fidelity in sensitivity to the antiviral agent.
102

RESULTS

Viable CVB3-K159 mutants acquired the A239G mutation in the RdRp

Low-level T-705-resistant CHIKV variants were reported to have the K291R mutation in motif F1 of the RdRp (9). Because this lysine residue is highly conserved in the RdRp of +ssRNA viruses (**Figure 1**), we introduced the K-to-R mutation at the corresponding position in motif F1 of the CVB3 RdRp (K159R) to assess the sensitivity of this mutant to the antiviral effect of T-705 (**Figure 2**). Initially, no infectious virus could be recovered. However, during the second transfection round, virus-induced CPE was observed and infectious virus was recovered. Sequencing of this virus sample revealed that, in addition to the engineered K159R, it had also acquired the Alanine to glycine substitution at position 239 in motif A of the RdRp (**Figure 2**). Interestingly, the single A239G mutant has been reported to be a low fidelity RdRp CVB3 variant (13).

To explore the importance of the lysine at position 159 in the CVB3 RdRp, a full set of mutations was engineered, each coding for another amino acid residue at this position. From nine of these infectious clones, no virus could be recovered from cell culture after two transfection rounds and no RNA replication could be detected, requiring them to be labeled as 'not viable'. Another eight mutants reverted back to WT (**Table 1**). Only transfection with the K159M clone allowed recovering infectious virus with a mutation at position 159, however only after it had acquired the A239G substitution (**Table 1**). The low fidelity RdRp variant (A239G) (13) and a high fidelity RdRp variant (A372V) (14) were also generated to be used as controls in the next experiments.

K159 mutations in the CVB3 RdRp gene affect polymerase competence

An enzymatic study was performed to determine how the K159 mutations affect RdRp activity. The *in vitro* polymerase assays were performed with purified CVB3 RdRp and a homo-polymeric primer-template substrate (**Figure 3A**) allowing [α-32P]-UMP incor-

poration into RNA after 2, 5 and 10 min. Relative to WT polymerase, the single K159R and K159M variants showed significant differences of overall 100- and 15-fold decrease in polymerase activity, respectively (**Figure 3B/C**). Interestingly, introduction of the A239G mutation **partially restored** the overall polymerase activity of both K159 mutants (**Figure 3B/C**). Based on structural analysis of the picornavirus CVB3 (PDB code 3CDW), the Arg159 has a long side-chain compared to Lys159, which narrows the access of the incoming nucleotides and impedes correct positioning at the active site of the RdRp (**Figure 4B/E**). This may explain the lower efficiency noted in polymerase activity assays. In the case of Met159, it is suggested that the nitrogen group of the original lysine residue has a main role in the binding and positioning of the incoming nucleotide and its substitution by a methyl group in methionine may therefore affect directly the NTP recognition and in turn NTP-positioning and catalysis. As shown in (**Figure 4A/D**), the residues Lys159 and Ala239 are spatially close in the channel of the incoming NTP. This channel becomes narrow when the Lys159 is mutated thereby hindering the access of the incoming NTP to the RdRp active site (**Figure 4B/E**). In order to maintain virus viability, the compensatory mutation A239G, with its absence of side-chain, appears to restore the open conformation of the NTP channel (**Figure 4C/F**).These data are in agreement with the fact that no viable single mutant viruses could be recovered after transfection in cell culture, and that the A239G mutation was spontaneously acquired by the K159R and K159M mutants to restore their ability to replicate *in vitro*.

The K159R/M mutations result in an unfavorable phenotype

The genetic stability of the amino acid substitutions of the K159R-A239G and K159M-A239G mutants was studied during passaging in HeLa Rh cells. Already after three passages, both K159 mutants had reverted back to the WT lysine. The adaptive mutation at

position 239 appeared to be genetically stable, with or without the substitutions at position 159 (**Table 2**).

Plaque phenotyping of the reverse-engineered K159 mutants before passaging revealed that the plaque size of the K159M-A239G variant was comparable to that of WT, whereas for the K159R-A239G variant, two populations with different plaque size were observed (**Figure 5A**). Despite numerous attempts, it was not possible to obtain a pure small-plaque variant. In parallel, the *in vitro* growth kinetics of all variants were determined in Vero A cells by plaque assay. The A239G and K159R-A239G variants had slightly slower growth kinetics compared to WT virus, whereas the K159M-A239G mutant replicated approximately as efficiently as WT (**Figure 5B**).

CVB3-K159 mutants are more susceptible to the antiviral effect of T-705

The susceptibility to the antiviral effect of T-705 (**Figure 6**) of WT virus as well as of RdRp mutants was quantified in a CPE reduction assay (**Figure 5C**). The K159R-A239G and K159M-A239G mutants proved to be respectively 3.4- and 2-fold more susceptible to the antiviral effect of T-705 than WT virus (**Table 3**). Also the single A239G mutant proved to be 2-fold more susceptible, whereas the high fidelity polymerase variant A372V was 2-fold less sensitive to T-705 than WT. The susceptibility of the K159 variants to the antiviral effect of ribavirin (which acts as a mutagenic agent and by depletion of GTP pools) (15) and rupintrivir (an inhibitor of the viral 3C protease) was not significantly altered (**Table 3, Figure 6**).

K159 mutations affect polymerase fidelity

Because low and high fidelity variants of the RdRp (A239G and A372V) exhibited a different susceptibility to T-705, *in vitro* polymerase assays were performed to assess the effect of the K159 mutations on polymerase fidelity (**Figure 7**). In these enzymatic assays, insertion of the correct nucleotide (UTP) into RNA was challenged with increasing

concentrations of an incorrect (CTP) nucleotide. The low polymerase efficiency of single K159R and K159M variants technically precluded their use in fidelity analysis assays. The A239G variant was used as low fidelity control (13, 14). The RNA product formed was quantified and fit as a dose-response curve framing the incorrect nucleotide concentration able to inhibit 50% of RNA product formation (reported as IC_{50}). For WT, A239G, K159R-A239G and K159M-A239G, an IC_{50} of 2.9 ± 0.2 mM (**Figure 7A/B**), 2.5 ± 0.3 mM (**Figure 7A/C**), 1.7 ± 0.06 mM (**Figure 7A/D**) and 0.45 mM ± 0.04 (**Figure 7A/E**) were obtained when 3 μCi [α-^{32}P]-UTP / 10μM unlabeled UTP was challenged with different concentrations of CTP, respectively. Altogether, these results indicate that the K159R-A239G and K159M-A239G variants are respectively 1.7- and 6-fold more sensitive than the WT enzyme to the presence of an incorrect CTP nucleotide (**Figure 7F**). These results validate the hypothesis that the variants are indeed affected in their fidelity of nucleotide selection or incorporation. Because loss of fidelity would also favor incorporation of T-705-RTP, these results are in agreement with the observation that the K159 variants are more susceptible to the antiviral effect of this compound.

T-705 acts as a mutagen during CVB3 replication

To study whether T-705 acts as a mutagen on CVB3 replication, virus-infected HeLa Rh cells were treated with T-705 or ribavirin at a concentration equal to the EC_{50} of the corresponding compound (**Table 3**). This study was performed with the WT virus, the low fidelity A239G as well as the high fidelity A372V variant because, as demonstrated above, the K159 mutants easily revert back to WT, which would interfere with data analysis. On day 3 post-infection (p.i.), the supernatants were collected and subjected to deep sequencing to determine the mutation frequencies at each nucleotide position after drug treatment. As expected, the high fidelity A372V variant (**Figure 8B, data representing open bars**) has a significantly lower mean basal mutation frequency across its

genome [P<0.0001, paired two-tailed t-test, n=10,749] than the WT virus (**Figure 8A, data representing open bars**) whereas the low fidelity A239G variant showed the highest mean basal mutation frequency across its genome frequencies [P<0.0001, paired two-tailed t test, n=10,749] (**Figure 8C, data representing open bars**). Treatment with T-705 (**Figure 8, light grey bars**) and ribavirin (**Figure 8, dark grey bars**) resulted in a significantly higher basal mutation frequency for all CVB3 variants. The data demonstrate that T-705 is a potent RNA mutagen for CVB3, especially for C->U and G->A transitions, as has been previously described (16, 17). On the other hand, ribavirin increased the mutation frequency for all transition mutations.

The K159R-A239G mutant is attenuated *in vivo*

The fitness of CVB3 WT as well as the A239G, K159R-A239G and K159M-A239G mutants was studied in immunocompetent SJL mice. The A239G variant was included as a control for *in vivo* attenuation (13). Three days p.i., a time at which the highest virus titers are observed in the WT-infected mice, all mice were euthanized and serum, heart, spleen and pancreas were collected for RNA quantification (**Figure 9**). Mice infected with the A239G mutant had lower RNA levels in the serum and various organs than WT (**Figure 9A-D**) as well as less infectious virus particles in the heart (**Figure 9E**), which is in agreement with previous reports. The K159R-A239G mutant was the most attenuated variant in this study inducing only low or undetectable levels of viral RNA in the heart (**Figure 9B**). Furthermore, no infectious virus particles were recovered from this organ (**Figure 9E**) in which CVB3 typically replicates to high titers. In contrast, the K159M-A239G variant behaved comparable to WT (**Figure 9A-E**). Sequencing of the virus population in serum samples of mice infected with the K159M-A239G variant revealed that this variant had reverted back to WT.

Discussion

T-705 is a broad-spectrum antiviral compound that has been reported to inhibit the replication of a variety of RNA viruses, both in *in vitro* and *in vivo* models. In a previous study, CHIKV variants that are resistant to the antiviral activity of T-705 were selected and all of them were shown to have acquired the K291R mutation in motif F1 of the RdRp (9). Because this lysine residue is highly conserved in the RdRp of many different +ssRNA viruses, we hypothesized that this residue is essential for the polymerase activity of these viruses and that it is a key interactor with T-705-RTP. To challenge this hypothesis, the K-to-R mutation was inserted at the equivalent position (K159R) in the infectious clone of CVB3. In parallel, two different resistance selection protocols (serial passaging and clonal selection) were used with the aim to select T-705-resistant CVB3 variants. However, despite numerous attempts, we did not succeed to select such variants, indicating a high barrier to resistance of T-705. In contrast to the CHIKV RdRp, the CVB3 RdRp did not tolerate this mutation without the presence of the compensatory A239G amino acid substitution in motif A of the RdRp. Interestingly, a CVB3 variant carrying the single A239G mutation was previously reported to be a low fidelity polymerase variant (13). Of all CVB3 infectious clones carrying any possible amino acid substitution at position 159, only the K159M variant proved to be viable and this only after the A239G mutation had also been **acquired. Interestingly**, *in vitro* polymerase assays revealed that the K159R and K159M mutants exhibit crippled polymerase activity, which can be efficiently restored by the compensatory A239G substitution. As mentioned before, the Lys159 residue is located in Motif F of the RdRp, which has been reported to play an important role in NTP binding during viral RNA synthesis (10). NTP binding is known to be a major fidelity checkpoint and point mutations in this motif could anhilate polymerase activity or slow down catalysis (18). Mutating this lysine residue to an argi-

nine or methionine resulted in reduced polymerization efficiency which is likely the consequence of less efficient access of the incoming NTPs to the active site of RdRp. According to previous reports (19, 20), the residue Ala239 participate in a tetrahedral hydrogen bond network. This network helps position the Asp238 residue to the active site of the RdRp, providing a direct link between the properly positioned NTP and a set of structural interactions that promote catalysis by stabilizing the closed active site (18). Based on structural analysis of CVB3 polymerase, the residues Lys159 and Ala239 are closely located in the channel of the incoming NTP. This channel becomes narrow when the Lys159 is mutated to a slightly bulkier R or M which is expected to impede access of the incoming NTP to the RdRp active site. With the "removal" of the methyl side-chain, the compensatory mutation A239G, appears to restore the access to the NTP channel. Consequently, the overall polymerase activity and the ability of the virus carrying this compensatory mutation to replicate *in vitro* is restored. These data indicate first of all that the K159 residue is of key importance for the catalytic activity of the CVB3 RdRp and secondly that the residue at position 239 has an important role in its stability. Surprisingly, the K159R-A239G and K159M-A239G variants proved respectively 3.5- and 2-fold more sensitive (instead of resistant) to the antiviral activity of T-705 when compared to WT. In contrast, no significant differences in sensitivity to ribavirin and rupintrivir were observed, indicating that the K159 residue is specifically involved in the molecular mechanism of action of T-705. Furthermore, also the low fidelity A239G variant was more sensitive to the antiviral effect of T-705, whereas the high fidelity variant A372V proved less sensitive. These data thus indicate that the fidelity of the viral RdRp is an important component in the susceptibility of the virus to T-705. Therefore, *in vitro* polymerase studies were performed to evaluate the fidelity of the K159 mutants. The K159R-A239G and K159M-A239G variants were respectively 1.7- and 6-fold more sensi-

276 tive than the WT enzyme to the presence of an incorrect nucleotide and their fidelity
277 was lower than that of the single A239G mutant. This provides an explanation for the
278 increased sensitivity of the double mutants to the antiviral activity of T-705.

279 To date, the precise mechanism that underlies the broad-spectrum anti-RNA virus activ-
280 ity of T-705 has not been completely unraveled. T-705 is converted intracellularly into
281 its T-705-RTP form, which behaves as a pseudo-purine (21, 22). Consequently, incorpo-
282 ration of T-705-RTP into the viral RNA by the RdRp may possibly lead to chain termina-
283 tion or lethal mutagenesis. Some studies support lethal mutagenesis as the mechanism
284 of action of T-705, for example against influenza virus (8) and norovirus (7). It was also
285 reported that the incorporation of T-705-RTP by the norovirus RdRp does not result in
286 complete chain termination (23). On the other hand, two studies have shown that in-
287 corporation of either a single (6) or two consecutive T-705-RTP molecules (24) into the
288 nascent influenza viral RNA strand prevents further RNA strand extension. Moreover,
289 we demonstrated earlier that the reduction of CHIKV RNA titers by T-705 correlates
290 well with a decrease in infectivity, suggesting that lethal mutagenesis is probably not
291 the mechanism of the antiviral effect of T-705 against CHIKV (9). By deep sequencing,
292 we here determined the mutation frequency in the genome of CVB3 that had been cul-
293 tured in the presence of T-705. Indeed, the mutation frequency in presence of ribavirin
294 was increased for all transition mutations; while T-705 had little effect on A->G and U-
295 >C transitions, but significantly increased C->U and G->A mutations between 3- and 10-
296 fold.

297 In a previous study, low RdRP fidelity variants of CVB3, such as the A239G variant, were
298 shown to be attenuated in immune-competent mice (13). Therefore, the fitness of the
299 reverse-engineered K159 mutants was studied in immune-competent SJL mice. The
300 A239G variant was included in the study as a positive control for *in vivo* attenuation.

Interestingly, the K159R-A239G variant had significantly lower viral RNA levels in serum and sampled organs, and failed to efficiently infect the heart. In contrast, the infectivity of the K159M-A239G variant was comparable to that of WT. However, sequencing of the collected samples revealed that the K159M-A239G variant completely reverted to WT in infected mice, providing an explanation for the above observation.

To conclude, the conserved lysine residue of the F1 RdRp motif was shown to be key for the antiviral activity of T-705 against both CHIKV and CVB3 and is most likely also a key element in the interaction of T-705 with the RdRp of other +ssRNA viruses. In addition, this lysine is crucial for the proper functioning of the RdRp which explains most likely the high barrier for antiviral resistance. Moreover, we demonstrate for the first time the role of RdRp fidelity in the mechanism of CVB3 sensitivity for T-705. These results provide more insights into the mechanism of the antiviral activity of T-705 and may help to design novel broad-spectrum +ssRNA virus inhibitors that target this particular region of the RdRp.

MATERIALS AND METHODS

Cells, viruses and inhibitors

Vero A cells (ATCC CCL-81) and HeLa Rh cells [kindly provided by K. Andries, Janssen Infectious Diseases, Belgium]were maintained in minimal essential medium (MEM Rega-3, Gibco) supplemented with 10% fetal bovine serum (FBS, Gibco), 1% L-glutamine (Gibco) and 1% sodium bicarbonate (Gibco). Virus propagation and antiviral assays were performed in the same medium but supplemented with 2% instead of 10% FBS. All cell cultures were maintained at 37°C in an atmosphere of 5% CO_2 and 95%-99% relative humidity.

T-705 was purchased from BOC Sciences (USA). Ribavirin (Virazole) was purchased from Valeant Pharmaceuticals International (Costa Mesa, CA). Rupintrivir was purchased from Axon Medchem (The Netherlands). Compounds were dissolved in DMSO to yield 10 mg/ml stock solutions and were stored at 4°C until used.

The CVB3 Nancy infectious cDNA clone was kindly provided by prof. F. van Kuppeveld, [University of Utrecht, The Netherlands].

Generation of CVB3 mutants

A full set of CVB3 mutants at position 159 of the RdRp gene were constructed by introducing the desired mutation in the CVB3 Nancy infectious cDNA clone or in the CVB3 RdRp-pASK3 plasmid in case of prokaryotic protein expression using the QuikChange mutagenesis kit (Agilent) and the primers described in **Table 4**. The identity of the mutation in each of the constructs was verified by Sanger sequencing using the BigDye® Terminator v3.1 Cycle Sequencing kit (Applied Biosystems) and a 3130 Genetic Analyzer automatic sequencer (Applied Biosystems). Subsequently, the mutated CVB3 infectious clones were *in vitro* transcribed into RNA using the RiboMAX™ Large Scale RNA Production System-T7 (Promega). An appropriate amount of *in vitro* transcribed RNA was

transfected into Vero A cells using the DMRIE-C reagent (Invitrogen). Following incubation for 3 days at 37°C, the cultures were inspected for cytopathic effects (CPE). The cultures with clear CPE were used to prepare virus stocks and stored at -80°C. From the cultures for which no CPE could be detected, the cells were harvested using Cells-to-cDNA™ lysis buffer (Life Technologies) for extraction of intracellular RNA and quantitative RT-PCR was performed to detect the presence of any replicating virus. In the case no viral RNA could be detected, the transfection procedure was repeated once more. A virus variant was considered 'not viable' when this second round also did not yield a positive PCR signal.

Sanger Sequencing

To confirm the presence of the introduced mutation in the reverse-engineered viruses, viral RNA was extracted using the NucleoSpin® RNA isolation kit (Macherey-Nagel). This RNA was used to generate five cDNA fragments that represent the entire coding region by RT–PCR amplification using the OneStep RT-PCR kit (Qiagen). These fragments were purified using the Wizard® SV Gel and PCR Clean-Up System (Promega), and sequenced on both strands (BigDye® Terminator v3.1 Cycle Sequencing kit). The complete nucleotide sequences were assembled in Contig Express (VNTI, Invitrogen) and the genomes of the different variants were compared to the wild-type genome.

Quantitative RT-PCR

One-step quantitative RT-PCR was performed using the ABI 7500 Fast Real-Time PCR System (Applied Biosystems, USA). The sequences of primers and probe and the thermal cycling conditions used in qRT-PCR were as described before (25). The RNA copy number in each sample was determined by a standard curve using serial dilutions of CVB3 standard cDNA included in the run.

Protein expression and purification

The CVB3 RdRp-pASK3 plasmid used in this study is a bacterial expression vector, which does not use bacteriophage T7 RNA polymerase. It was generated by cloning the region encoding CVB3 RdRp from the CVB3 Nancy infectious cDNA clone into the prokaryote expression vector pASK3 (IBA) by PCR using two primers (forward 5'-GGAATTCTAAGGAGGTAGAACCATGGGTGAAATAGAATTTATTGAGAGC-3'; reverse 5'-CCGCCGCTCGAGTTAATGGTGATGGTGATGGTGAAAGGAGTCCAACCACTTCCTG-3'). The CBV3 RdRp contains a 6-histidine tag in the C-terminal end.

E. coli strain Rosetta 2 cells (Novagen), transformed with the CVB3 RdRp-pASK3 WT or variant plasmids, were grown in LB medium at 37°C and induced overnight with 200 µg/L anhydrotetracycline when the OD_{600} (optical density) value reached 0.6. Expression was performed at 17°C for 16h in light-protected conditions. Soluble fraction and metal–ion affinity chromatography (IMAC) purification step were performed as described previously (26). The pure fractions analyzed on the SDS-PAGE gel were pooled, dialyzed into 20 mM Tris pH 9, 300 mM NaCl, 5% glycerol and 0.5 mM Tris (2-carboxyethyl) phosphine hydrochloride (TCEP-HCl, Sigma) and concentrated using Centricon (Millipore) concentrators (30 kDa molecular weight cutoff). All proteins were stored at -20°C in cryoprotecting conditions using 50% glycerol.

In vitro polymerase assays

RNA oligo (dT) primers of 15 nucleotides (nt) and poly(rA) templates of approximately 357nt in length were used for elongation assays in an analogous system as previously described (27, 28). Primers and templates were purchased from Thermo Fisher Scientific and Amersham Pharmacia Biotech, respectively. Both were mixed for annealing at a molar ratio of 1:2 (template/primer) in the presence of water. The mixtures were incu-

388 bated at 70°C during 10 min and cooled down slowly to room temperature and then left
389 stored at -20°C until further use.
390 *In vitro* enzymatic assays were carried out using polymerase assay buffer (20 mM Hepes
391 pH 7.5; 50 mM KCl; 5 mM DTT; 5 mM $MgCl_2$) mixed with 1 μM CVB3 RdRp and 0.5 μM
392 pre-annealed primer-template substrate in 10 μL of reaction. Thus, the polymerase and
393 its RNA substrate were assembled at 30°C for 15 min to perform an active elongation
394 complex. The primer extension was started by the addition of a mixture of 3 μCi [α-^{32}P]-
395 UTP and 10 μM of UTP unlabeled using the same polymerase assay buffer in an equal
396 volume of reaction. In the case of competition assays, CTP was added at concentrations
397 of 1, 2, 3, 4, or 5 mM for WT and A239G variants. In the case of K159R-A239G and
398 K159M-A239G variants, concentrations were adjusted to 0.1, 0.25, 0.5, 1, or 2 mM of
399 CTP. NTPs were purchased from GE Healthcare.
400 After incubation at 30°C, aliquots of reactions were quenched at various time points by
401 the addition of an equal volume of loading buffer (formamide with 10 mM EDTA). Reac-
402 tion products were analyzed by PAGE using polyacrylamide sequencing gels of 14%
403 acrylamide:bisacrilamide (19:1), 7 M urea with TTE buffer (89 mM Tris pH 8.0, 28 mM
404 taurine (2-aminoethanesulfonic acid), 0.5 mM EDTA). RNA bands were visualized using
405 a Fluorescent Image Analyzer FLA3000 (Fuji), and quantified using Image Quant Soft-
406 ware (Fuji).
407 **CPE reduction assay**
408 HeLa Rh cells were seeded in 96-well tissue culture plates (BD Falcon) at a density of 1.8
409 $\times 10^4$ cells/well and were allowed to adhere overnight. The next day, 2-fold dilution se-
410 ries of T-705, ribavirin or rupintrivir (starting concentration 637, 819 and 8 μM, respec-
411 tively) were added to the cultures that were then infected with the selected CVB3 vari-
412 ant at a final multiplicity of infection (MOI) of 0.001 PFU/cell. At day 3 post-infection

413 (p.i.), the antiviral effect was quantified using the MTS/PMS method as described by the
414 manufacturer (Promega, The Netherlands). The 50% effective concentration (EC_{50}),
415 which is defined as the concentration of compound that is required to inhibit virus-
416 induced cell death by 50%, was determined using logarithmic interpolation.

417 **Genetic stability of the generated mutants**

418 To assess the genetic stability of the reverse-engineered mutations, HeLa Rh cells were
419 seeded at a density of $4x10^4$ cells/well in 48-well plates and infected with the selected
420 CVB3 variant at a MOI=0.01. Each variant was passaged 3 times after which the appro-
421 priate region of the RdRp was sequenced.

422 **Virus phenotyping**

423 Vero A cells were seeded in 6-well plates (BD Falcon) at a density of $1×10^6$ cells/well.
424 Following 24h of incubation, cells were washed with PBS and then infected with 10-fold
425 serial dilutions of the respective virus stock. After 2h of incubation with gentle shaking,
426 the monolayers were washed with PBS after which a freshly prepared 1:1 mixture of
427 liquefied 1% low melting point agarose (Invitrogen) and 2x medium with 4% FBS was
428 added. On day 3 p.i., the monolayers were carefully washed with PBS, fixed with 4%
429 formaldehyde and stained with Giemsa solution to visualize the virus-induced plaques,
430 after which they were counted to calculate the number of plaque forming units (pfu) per
431 mL.

432 In parallel, the growth kinetics of different CVB3 mutants were determined by infecting
433 Vero A cells ($5×10^4$ cells/well) in 96-well plates with the respective virus variants at a
434 MOI of 3. After 1h of infection, the cells were washed with assay medium to remove non-
435 adsorbed virus. At 4, 6, 8, 10, 12 and 24h p.i., the culture supernatant was collected, after
436 which the infectious virus content was quantified by plaque assay as before.

437 **The effect of T-705 on the mutation frequency of CVB3 by deep sequencing**

HeLa Rh cells were seeded in a 48-well plate at a cell density of 4×10^4 cells/well and were left to adhere overnight. Next day, cells were treated with T-705 or ribavirin at a final concentration that equals the EC_{50} value against the tested variant. Cells were then infected with CVB3 WT, A239G or A372V at a final MOI=0.001. On day 3 p.i., the culture supernatant in each well was collected and the virus populations in these samples were subjected to a deep sequencing study. Samples were RNA extracted using Trizol and RT-PCR amplified by RT (Superscript III) and PCR (Phusion) using primers sets that covered the whole genome in 3-4 kb fragments. PCR fragments were purified via the Nucleospin Gel and PCR Clean-up kit (Macherey-Nagel). PCR products were then fragmented (Fragmentase), linked to Illumina multiplex adapters, clustered and sequenced with NextSeq500 technology. Sequences were demultiplexed by CASAVA with no mismatches permitted. Clipping was performed using the fastq-mcf tool (http://code.google.com/p/ea-utils/wiki/FastqMcf), removing common adapter contaminants and trimming low quality bases (Phred<30). Clipped reads were aligned to the CVB3 Nancy sequence as reference with a maximum of 2 mismatches per read, and no gaps, using BWA v0.5.9. Alignments were processed using SAMTools to obtain a pile-up of the called bases at each position. The ViVAn pipeline was used to identify statistically significant variants above the background noise due to sequencing error, in every sufficiently covered site (>1000X) (29). Briefly, for each position throughout the viral genome, base identity and their quality scores were gathered. Each variant was determined to be true using a generalized likelihood-ratio test and its allele rate was modified according to its covering read qualities based on a maximum likelihood estimation. Additionally, a confidence interval was calculated for each allele rate. To correct for multiple testing, Benjamini-Hochberg false-discovery rate of 5% was set. The frequency of

transition mutations for compound-treated samples was determined at each position across the genome and compared to untreated controls in a two-tailed paired t-test.

In vivo experiments

SJL mice were bred in the Experimental Animal Breeding Facility of the University of Leuven, Belgium. Four groups of SJL mice (5 animals/group) were used. Mice were infected with 10^5 PFU of the selected CVB3 variant (WT, K159R-A239G, K159M-A239G or A239G) by i.p. injection (200 µl). On day 3 p.i., all animals were euthanized and serum, heart, spleen and pancreas were collected. The viral RNA was isolated from serum using the NucleoSpin® RNA isolation kit (Macherey-Nagel) and from the homogenized organs using the RNeasy Mini Kit (Qiagen). The amount of viral RNA in serum and organs was then quantified by qRT-PCR as described before. In addition, the number of infectious virus particles in the heart was determined by end-point titration in Vero A cells.

Ethics Statement

The *in vivo* experiments were performed according to the Belgian guidelines for animal experimentation and with the authorization of the Ethical Committee of University of Leuven (KUL), Belgium (P080-2015).

Acknowledgements

We thank Barbara Selisko for helpful discussions and help in the initial phase of this project, François Ferron for help in the analysis of polymerase structures, and Carolien De Keyzer for the excellent technical support in the animal experiments.

Funding

This work was supported by BELVIR project from BELSPO (IUAP), the EU-FP7/2011-2014 Project SILVER (GA 260644), and the EU-H2020 Innovative Training Network ANTIVIRALS (GA 642434). A.T.S.M. was supported by a postdoctoral fellowship from CNPq (Conselho Nacional de Desenvolvimento Cientifico e Tecnologico – Brasil). L.D. was supported by a post-doctoral fellowship from the FWO (Fund for Scientific Research of Flanders, Belgium).

Conflict of interest

The authors declare no conflict of interest.

References

1. **Furuta Y**, **Gowen BB**, **Takahashi K**, **Shiraki K**, **Smee DF**, **Barnard DL**. 2013. Favipiravir (T-705), a novel viral RNA polymerase inhibitor. Antiviral Res **100**:446–454.
2. **Rocha-Pereira J**, **Jochmans D**, **Dallmeier K**, **Leyssen P**, **Nascimento MSJ**, **Neyts J**. 2012. Favipiravir (T-705) inhibits in vitro norovirus replication. Biochem Biophys Res Commun **424**:777–780.
3. **Zmurko J**, **Marques RE**, **Schols D**, **Verbeken E**, **Kaptein SJF**, **Neyts J**. 2016. The Viral Polymerase Inhibitor 7-Deaza-2'-C-Methyladenosine Is a Potent Inhibitor of In Vitro Zika Virus Replication and Delays Disease Progression in a Robust Mouse Infection Model. PLoS Negl Trop Dis **10**.
4. **Safronetz D**, **Falzarano D**, **Scott DP**, **Furuta Y**, **Feldmann H**, **Gowen BB**. 2013. Antiviral efficacy of favipiravir against two prominent etiological agents of hantavirus pulmonary syndrome. Antimicrob Agents Chemother **57**:4673–4680.
5. **Mentré F**, **Taburet A-M**, **Guedj J**, **Anglaret X**, **Keïta S**, **de Lamballerie X**, **Malvy D**. 2015. Dose regimen of favipiravir for Ebola virus disease. Lancet Infect Dis **15**:150–151.
6. **Sangawa H**, **Komeno T**, **Nishikawa H**, **Yoshida A**, **Takahashi K**, **Nomura N**, **Furuta Y**. 2013. Mechanism of Action of T-705 Ribosyl Triphosphate against Influenza Virus RNA Polymerase. Antimicrob Agents Chemother **57**:5202–5208.
7. **Arias A**, **Thorne L**, **Goodfellow I**. 2014. Favipiravir elicits antiviral mutagenesis during virus replication in vivo. Elife **3**:1–15.
8. **Baranovich T**, **Wong S-S**, **Armstrong J**, **Marjuki H**, **Webby RJ**, **Webster RG**, **Govorkova E a**. 2013. T-705 (favipiravir) induces lethal mutagenesis in influenza A H1N1 viruses in vitro. J Virol **87**:3741–51.
9. **Delang L**, **Segura Guerrero N**, **Tas A**, **Quérat G**, **Pastorino B**, **Froeyen M**, **Dallmeier K**, **Jochmans D**, **Herdewijn P**, **Bello F**, **Snijder EJ**, **de Lamballerie X**, **Martina B**, **Neyts J**, **van Hemert MJ**, **Leyssen P**. 2014. Mutations in the chikungunya virus non-structural proteins cause resistance to favipiravir (T-705), a broad-spectrum antiviral. J Antimicrob

Chemother **69**:2770–84.

10. **Ferrer-Orta C**, **Agudo R**, **Domingo E**, **Verdaguer N**. 2009. Structural insights into replication initiation and elongation processes by the FMDV RNA-dependent RNA polymerase. Curr Opin Struct Biol **19**:752–8.

11. **Iglesias NG**, **Filomatori C V**, **Gamarnik A V**. 2011. The F1 motif of dengue virus polymerase NS5 is involved in promoter-dependent RNA synthesis. J Virol **85**:5745–56.

12. **Surana P**, **Satchidanandam V**, **Nair DT**. 2014. RNA-dependent RNA polymerase of Japanese encephalitis virus binds the initiator nucleotide GTP to form a mechanistically important pre-initiation state. Nucleic Acids Res **42**:2758–2773.

13. **Gnadig NF**, **Beaucourt S**, **Campagnola G**, **Borderia a. V.**, **Sanz-Ramos M**, **Gong P**, **Blanc H**, **Peersen OB**, **Vignuzzi M**. 2012. Coxsackievirus B3 mutator strains are attenuated in vivo. Proc Natl Acad Sci **109**:E2294–E2303.

14. **Levi LI**, **Gnädig NF**, **Beaucourt S**, **McPherson MJ**, **Baron B**, **Arnold JJ**, **Vignuzzi M**. 2010. Fidelity Variants of RNA Dependent RNA polymerases uncover an indirect, mutagenic activity of amiloride compounds. PLoS Pathog **6**:1–14.

15. **Paeshuyse J**, **Dallmeier K**, **Neyts J**. 2011. Ribavirin for the treatment of chronic hepatitis C virus infection: A review of the proposed mechanisms of action. Curr Opin Virol **1**:590–598.

16. **Vanderlinden E, Vrancken B, Van Houdt J, Rajwanshi VK, Gillemot S AG**, **Lemey P, Naesens L**. 2016. Distinct Effects of T-705 (Favipiravir) and Ribavirin on Influenza Virus Replication and Viral RNA Synthesis. Antimicrob Agents Chemother **60**:6679–6691.

17. **De Avila AI**, **Gallego I**, **Soria ME**, **Gregori J**, **Quer J**, **Ignacio Esteban J**, **Rice CM**, **Domingo E**, **Perales C**. 2016. Lethal mutagenesis of hepatitis C virus induced by favipiravir. PLoS One **11**:e0164691.

18. **Peersen OB**. 2017. Picornaviral Polymerase Structure, Function, and Fidelity Modulation. Virus Res **In Press**:1–17.

19. **Arnold JJ**, **Vignuzzi M**, **Stone JK**, **Andino R**, **Cameron CE**. 2005. Remote site control of an

active site fidelity checkpoint in a viral RNA-dependent RNA polymerase. J Biol Chem **280**:25706–25716.

20. **Thompson A a**, **Peersen OB**. 2004. Structural basis for proteolysis-dependent activation of the poliovirus RNA-dependent RNA polymerase. EMBO J **23**:3462–3471.

21. **Furuta Y**, **Takahashi K**, **Kuno-maekawa M**, **Sangawa H**, **Uehara S**, **Kozaki K**, **Nomura N**, **Egawa H**, **Shiraki K**. 2005. Mechanism of Action of T-705 against Influenza Virus Mechanism of Action of T-705 against Influenza Virus. Antimicrob Agents Chemother **49**:981–986.

22. **Naesens L**, **Guddat LW**, **Keough DT**, **van Kuilenburg ABP**, **Meijer J**, **Vande Voorde J**, **Balzarini J**. 2013. Role of human hypoxanthine Guanine phosphoribosyltransferase in activation of the antiviral agent T-705 (favipiravir). Mol Pharmacol **84**:615–29.

23. **Jin Z**, **Tucker K**, **Lin X**, **Kao CC**, **Shaw K**, **Tan H**, **Symons J**, **Behera I**, **Rajwanshi VK**, **Dyatkina N**, **Wang G**, **Beigelman L**, **Deval J**. 2015. Biochemical Evaluation of the Inhibition Properties of Favipiravir (T-705) and 2' -C-methyl-cytidine Triphosphates against Human and Mouse Norovirus RNA Polymerases. Antimicrob Agents Chemother **59**:7504–16.

24. **Jin Z**, **Smith LK**, **Rajwanshi VK**, **Kim B**, **Deval J**. 2013. The Ambiguous Base-Pairing and High Substrate Efficiency of T-705 (Favipiravir) Ribofuranosyl 5'-Triphosphate towards Influenza A Virus Polymerase. PLoS One **8**:e68347.

25. **De Palma AM**, **Thibaut HJ**, **Van Der Linden L**, **Lanke K**, **Heggermont W**, **Ireland S**, **Andrews R**, **Arimilli M**, **Al-Tel TH**, **De Clercq E**, **Van Kuppeveld F**, **Neyts J**. 2009. Mutations in the nonstructural protein 3A confer resistance to the novel enterovirus replication inhibitor TTP-8307. Antimicrob Agents Chemother **53**:1850–1857.

26. **Jabafi I**, **Selisko B**, **Coutard B**, **De Palma AM**, **Neyts J**, **Egloff MP**, **Grisel S**, **Dalle K**, **Campanacci V**, **Spinelli S**, **Cambillau C**, **Canard B**, **Gruez A**. 2007. Improved crystallization of the coxsackievirus B3 RNA-dependent RNA polymerase. Acta Crystallogr Sect F Struct Biol Cryst Commun **63**:495–8.

572 27. **Arnold JJ**, **Cameron CE**. 2000. Poliovirus RNA-dependent RNA polymerase (3D(pol)).
573 Assembly of stable, elongation-competent complexes by using a symmetrical primer-
574 template substrate (sym/sub). J Biol Chem **275**:5329–5336.
575 28. **Gong P**, **Campagnola G**, **Peersen OB**. 2009. A quantitative stopped-flow fluorescence
576 assay for measuring polymerase elongation rates. Anal Biochem **391**:45–55.
577 29. **Isakov O**, **Bordería A V.**, **Golan D**, **Hamenahem A**, **Celniker G**, **Yoffe L**, **Blanc H**,
578 **Vignuzzi M**, **Shomron N**. 2015. Deep sequencing analysis of viral infection and evolution
579 allows rapid and detailed characterization of viral mutant spectrum. Bioinformatics
580 **31**:2141–50.
581

582 **Figure legends**

583 **Figure 1. Multiple sequence alignment of Motif F1 of viral RdRp.** Part of the multiple
584 sequence alignment of RdRp of chikungunya virus (ACY09947.1), enteroviruses [Cox-
585 sacikevirus A21 (ABM54541.1), Coxsackievirus B3 (AAA74400.1), poliovirus type 1
586 (AAP37265.1), enterovirus D68 (AAR98503.1) and human rhinovirus B14
587 (NP_740525.1)], flaviviruses [Zika virus (AMO03410.1), Japanese encephalitis virus
588 (ABU94628.1)], murine norovirus (AEY83582.1) and hepatitis C virus (CAB46913.1)
589 that was generated using the PROMALS server
590 (http://prodata.swmed.edu/promals/promals.php). Motif F1 of the RdRp is indicated by
591 a black box and the residues corresponding to K291 in CHIKV are highlighted in yellow.

592 **Figure 2. Coxsackievirus B3 polymerase structure.** A) Structure of CVB3 polymerase
593 (PDB id: 4K4Y) showing the locations of Lys159 (K159) and Ala239 (A239) highlighted
594 in blue and magenta, respectively. B) Model of CVB3 polymerase structure (fingers =
595 blue, palm = green, thumb = red ribbons) with favipiravir triphosphate (T-705-RTP).
596 The primer RNA strand has a yellow ribbon, the template has a brown ribbon. T-705-
597 RTP has purple carbons. The complementary G is in cyan. The carbons of K159 and
598 A239 residues are highlighted in green. CVB3 hydrogen bonds from the sugar part of T-
599 705-RTP to the N-terminus (in cyan) via A239 (green carbons) are shown as black
600 dashed lines.

601 **Figure 3. Coxsackievirus B3 RdRp variants exhibit distinct polymerase activities.**
602 RNA polymerase assays were performed as described in the Methods section. A) dT15-
603 poly(rA) is an homopolymeric primer:template allowing the incorporation of [α-32P]-
604 UMP or UMP at the dT primer 3'-end. B) RNA products of a representative PAGE are
605 shown after at 2, 5 and 10 min of quenching. C) Quantified RNA products shown are
606 mean values ± SD of 2 independent experiments. Statistical analysis was performed

using two-way ANOVA in reference to WT for K159R or K159M (*p<0.05) ; to K159R for K159R-A239G (*p<0.05) ; or to K159M for K159M-A239G (*p<0.05).

Figure 4. Top view of the RdRp from CVB3 (PDB code 3CDW). A) The locations of the residues K159 and A239 are highlighted in purple and red, respectively. The channel from incoming rNTPs is shown between these residues. B) The long chain of the arginine residue, R159 mutant, is highlighted in purple narrowing the channel for incoming rNTPs. A239 is shown in red. C) The mutant G239, in red, is able to reestablish the access of rNTPs in the channel. The residue R159 is shown in purple. D-F) representative zoom of A to C, respectively.

Figure 5. Phenotype of reverse-engineered CVB3 variants. A) Plaque phenotypes of different CVB3 variants were determined by infecting Vero A cells with a 10-fold serial dilution of each variant followed by addition of an agarose overlay. After 3 days, viral plaques were visualized by Giemsa staining. A representative image with spread plaques is shown. **B)** Growth curves were generated by infecting Vero A cells with the selected CVB3 variant at a MOI of 3, after which the infectious virus titer in the medium was determined at various time points after infection by plaque assay. Infectious virus titer values are the mean ± SD of 2 independent experiments. Significant differences with respect to WT (*p<0.05 or ***p<0.001) were analyzed by two-way ANOVA. **C)** The sensitivity of the reverse-engineered CVB3 variants to the antiviral effect of T-705 was assessed in HeLa Rh cells by a CPE reduction assay. Cell viability was measured using the MTS/PMS method. Data are expressed as percentages of untreated controls and are mean values ± SD of at least 3 independent experiments.

Figure 6. **Chemical structure of favipiravir, ribavirin and rupintrivir**

Figure 7. K159R-A239G and K159M-A239G are low-fidelity RdRp variants. Competition assays were performed with 3 μCi [α-32P]-UTP/cold 10 μM UTP challenged with

CTP concentrations of 1, 2, 3, 4, 5 mM for (B) the wild-type and (C) A239G, or 0.1, 0.25, 0.5, 1, 2 mM for (D) K159R-A239G and (E) K159M-A239G variants. The total RNA products formed represents a mean ± SD of 2 independent experiments and was measured as a dose-response curve with at least one data point above and below 50% RNA product formed (A) to be able to calculate an interpolated apparent IC_{50} value. Data were fit (Figure 3F) and statistical analysis were performed using two-way ANOVA in reference to WT for K159R-A239G (*p<0.05) and for K159M-A239G (**p<0.01).

Figure 8. T-705 significantly increases the mutation frequency of CVB3. Wild-type **(A)**, high-fidelity A372V **(B)** and low-fidelity A239G **(C)** viruses were either mock-treated (open bars) or treated with T-705 (light grey bars) or ribavirin (dark grey bars), at concentrations equal to the corresponding EC_{50}, and subjected to whole-genome deep sequencing. The frequency of transition mutations occurring at each A, C, G, U was calculated and used to determine the mean frequency and SEM. *p<0.05, **p<0.01, ***p=0.0006, ****p<0.0001; two-tailed paired t-test; n=1416 (A->G), n=1169 (C->U); n=988 (G->A); n=1182 (U->C).

Figure 9. *In vivo* fitness of CVB3-K159 variants in SJL mice. SJL mice were infected with 10^5 PFU of CVB3 WT, A239G, K159R-A239G or K159R-A239G variants (n=5 per variant). On day 3 post infection, all mice were euthanized after which serum and selected organs were collected for RNA extraction. The amount of viral RNA in A) serum, B) heart, C) pancreas and D) spleen was determined by qRT-PCR. The number of infectious virus particles in the heart (E) was determined by end-point titration (*p<0.05 and **p<0.01, Kruskal-Wallis test).

Table 1. Mutation analysis of amino acid 159 of the CVB3 RdRp

Engineered genotype	Phenotype*	Compensatory mutation	$TCID_{50}$/ml	
			Vero A	HeLa Rh
Lys (wild-type)	Viable	-	2.2E+07	1.4E+05
Arg	Viable, but with	A239G	6.5E+06	1.9E+05
Met	Viable, but with	A239G	7.9E+07	2.5E+06
Asp	Reverted to WT	-	-	-
Asn	Reverted to WT	-	-	-
Gln	Reverted to WT	-	-	-
Ser	Reverted to WT	-	-	-
Thr	Reverted to WT	-	-	-
His	Reverted to WT	-	-	-
Phe	Reverted to WT	-	-	-
Val	Reverted to WT	-	-	-
Ala	Not viable	-	-	-
Ile	Not viable	-	-	-
Leu	Not viable	-	-	-
Trp	Not viable	-	-	-
Tyr	Not viable	-	-	-
Glu	Not viable	-	-	-
Cys	Not viable	-	-	-
Gly	Not viable	-	-	-
Pro	Not viable	-	-	-

**The phenotype indicates whether the transfected CVB3 variant with the desired mutation was viable, reverted to WT, or did not yield viable virus. Each transfection was performed at least in duplicate.*

659 **Table 2. Genetic stability of the reverse-engineered CVB3 variants in cell culture**

Engineered genotype	Genetic stability after 3 passages	
	Status*	**Genotype**
A372V	Stable	V372
A239G	Stable	G239
K159R-A239G	Partially stable	**K**159-G239
K159M-A239G	Partially stable	**K**159-G239

660 **The status indicates whether the mutations were stable, partially stable or reverted back*

661 *to WT over three passages in HeLa Rh cells.*

662 **Table 3. Antiviral activity of different classes of compounds against CVB3-K159**
663 **variants**

CVB3 variant	EC_{50} ± SD in µM (Fold of resistance)		
	T-705	Ribavirin	Rupintrivir
WT	229 ± 24	254 ± 37	0.6 ± 0.1
K159R-A239G	67 ± 6 **(0.3)******	261 ± 23	1 ± 0.4
K159M-A239G	116 ± 14 **(0.5)*****	198 ± 9	0.7 ± 0.1
A239G	108 ± 2 **(0.5) ******	164 ± 10 **(0.6)****	0.8 ± 0.02
A372V	458 ± 27 **(2) ******	419 ± 16 **(1.6)******	0.8 ± 0.01

664

665 *The values between brackets represent the fold of resistance (EC_{50} mutant/EC_{50} WT),*
666 *which have significant p-values (** p< 0.01, *** p< 0.001, **** p< 0.0001, Student T-*
667 *test).The 50% cytotoxic/cytostatic concentrations (CC_{50}) for T-705, ribavirin and rupin-*
668 *trivir were 1773 ± 9 µM, 914 ± 2 µM and >200 µM, respectively.*

669
670
671
672

673

674 **Table 4. CVB3 site-directed mutagenesis primers**

Mutation	Primer	Sequence (5'–3')	Length	Position	Tm
A239G	MFAT1	ttactctgggtacgatggtagcttaagccctgtctg	39	719	73.7
	MRAT1	cagacagggcttaagctaccatcgtacccagagtaa	39	719	73.7
A372V	MFAT2	gttacctggaccaacgtcactttcctaaagagg	33	1118	69.5
	MRAT2	cctctttaggaaagtgacgttggtccaggtaac	33	1118	69.5
K159R	MFAT3	ggtgacttatgtaagagatgagctcaggtc	30	479	66.8
	MRAT3	gacctgagctcatctcttacataagtcacc	30	479	66.8
K159M	MFAT4	ggtgacttatgtaatggatgagctcaggtc	30	479	66.8
	MRAT4	gacctgagctcatccattacataagtcacc	30	479	66.8

675

676

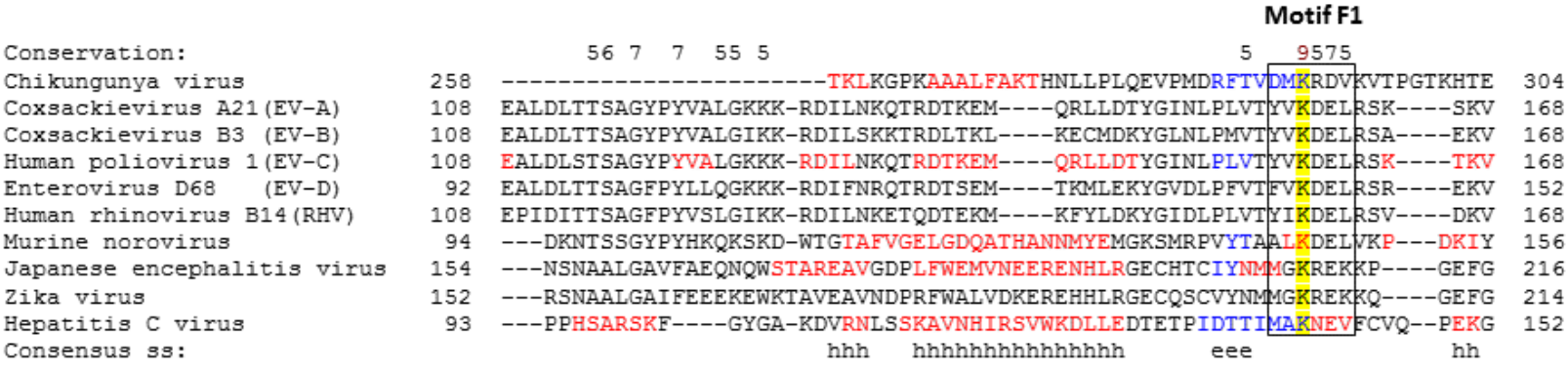
Motif F1
Conservation: 56 7 7 55 5 5 9575
Chikungunya virus 258 ----------TKLKGPKAAALFAKTHNLLPLQEVPMDRFTVDMKRDVKVTPGTKHTE 304
Coxsackievirus A21(EV-A) 108 EALDLTTSAGYPYVALGKKK-RDILNKQTRDTKEM----QRLLDTYGINLPLVTYVKDELRSK----SKV 168
Coxsackievirus B3 (EV-B) 108 EALDLTTSAGYPYVALGIKK-RDILSKKTRDLTKL----KECMDKYGLNLPMVTYVKDELRSA----EKV 168
Human poliovirus 1(EV-C) 108 EALDLSTSAGYPYVALGKKK-RDILNKQTRDTKEM----QRLLDTYGINLPLVTYVKDELRSK----TKV 168
Enterovirus D68 (EV-D) 92 EALDLTTSAGFPYLLQGKKK-RDIFNRQTRDTSEM----TKMLEKYGVDLPFVTFVKDELRSR----EKV 152
Human rhinovirus B14(RHV) 108 EPIDITTSAGFPYVSLGIKK-RDILNKETQDTEKM----KFYLDKYGIDLPLVTYIKDELRSV----DKV 168
Murine norovirus 94 ---DKNTSSGYPYHKQKSKD-WTGTAFVGELGDQATHANNMYEMGKSMRPVYTAALKDELVKP---DKIY 156
Japanese encephalitis virus 154 ---NSNAALGAVFAEQNQWSTAREAVGDPLFWEMVNEERENHLRGECHTCIYNMMGKREKKP----GEFG 216
Zika virus 152 ---RSNAALGAIFEEEKEWKTAVEAVNDPRFWALVDKEREHHLRGECQSCVYNMMGKREKKQ----GEFG 214
Hepatitis C virus 93 ---PPHSARSKF----GYGA-KDVRNLSSKAVNHIRSVWKDLLEDTETPIDTTIMAKNEVFCVQ--PEKG 152
Consensus ss: hhh hhhhhhhhhhhhhh eee hh

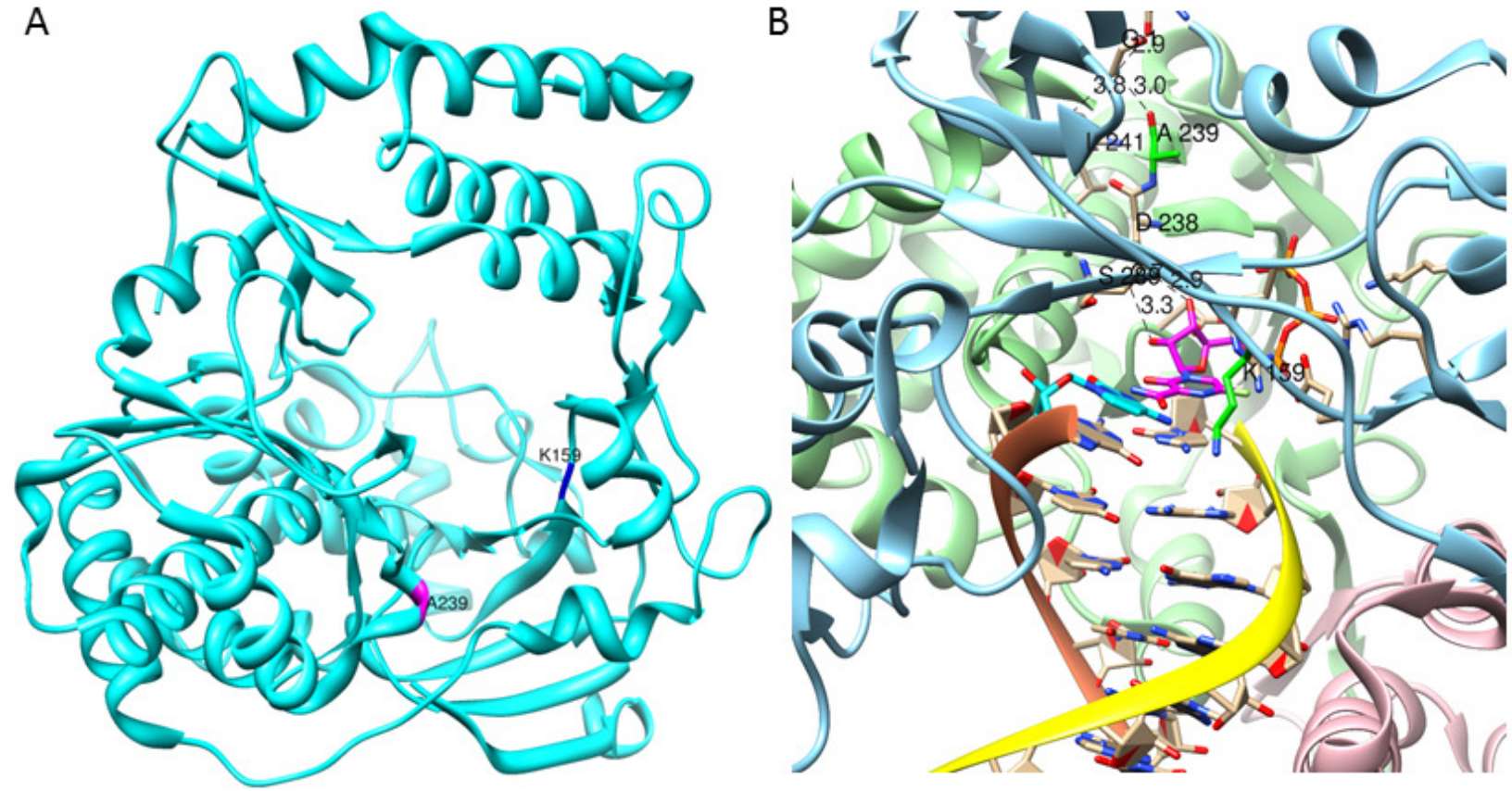
A
K159
A239
B
G 9
3.8 3.0
A 239
D 238
3.3

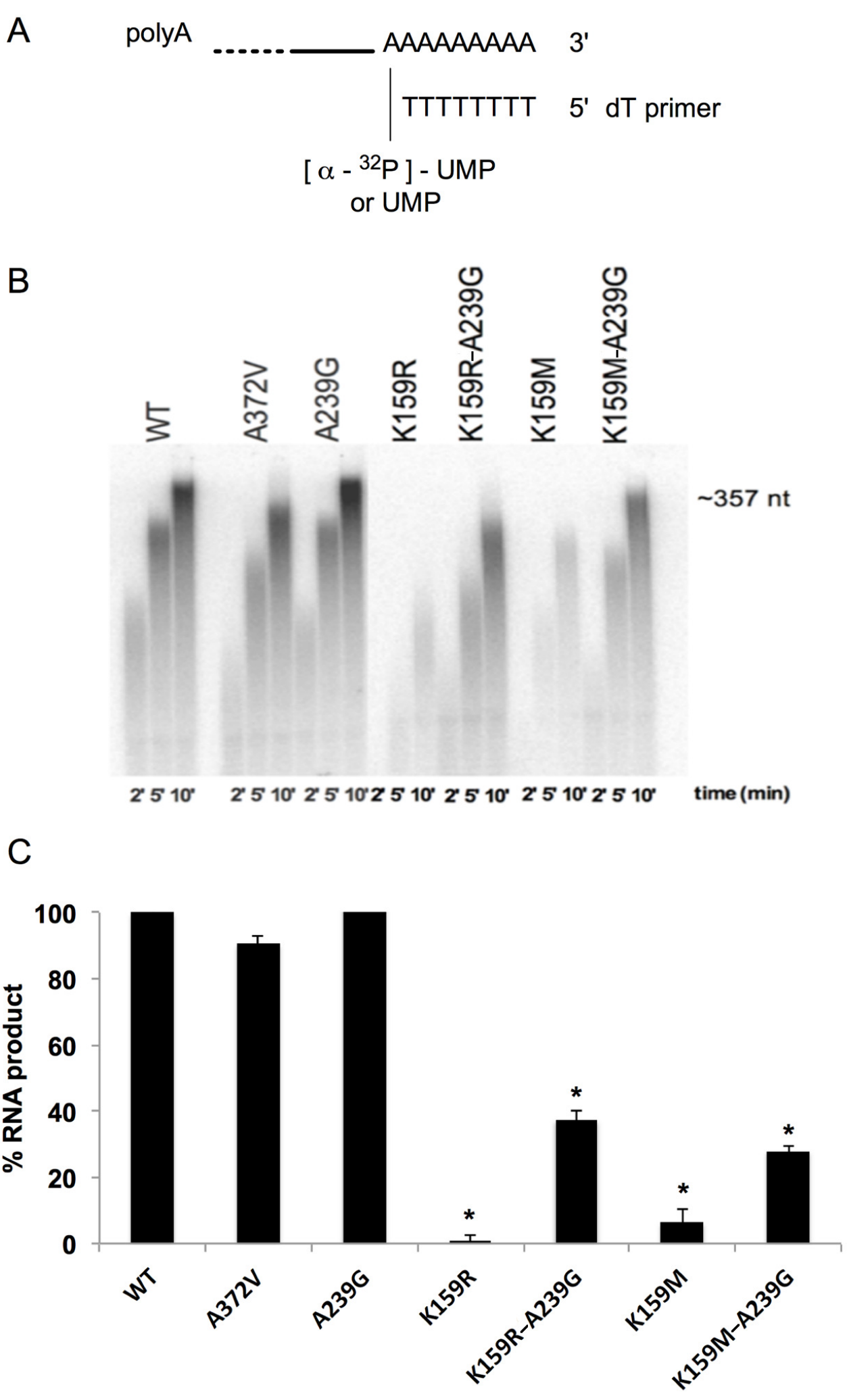
A
polyA
AAAAAAAAA 3'
TTTTTTTT 5' dT primer
[α - 32P] - UMP
or UMP
B
WT
A372V
A239G
K159R
K159R-A239G
K159M
K159M-A239G
~357 nt
2' 5' 10' 2' 5' 10' 2' 5' 10' 2' 5' 10' 2' 5' 10' 2' 5' 10' 2' 5' 10'
time (min)
C
% RNA product
100
80
60
40
20
0
WT
A372V
A239G
K159R
K159R-A239G
K159M
K159M-A239G

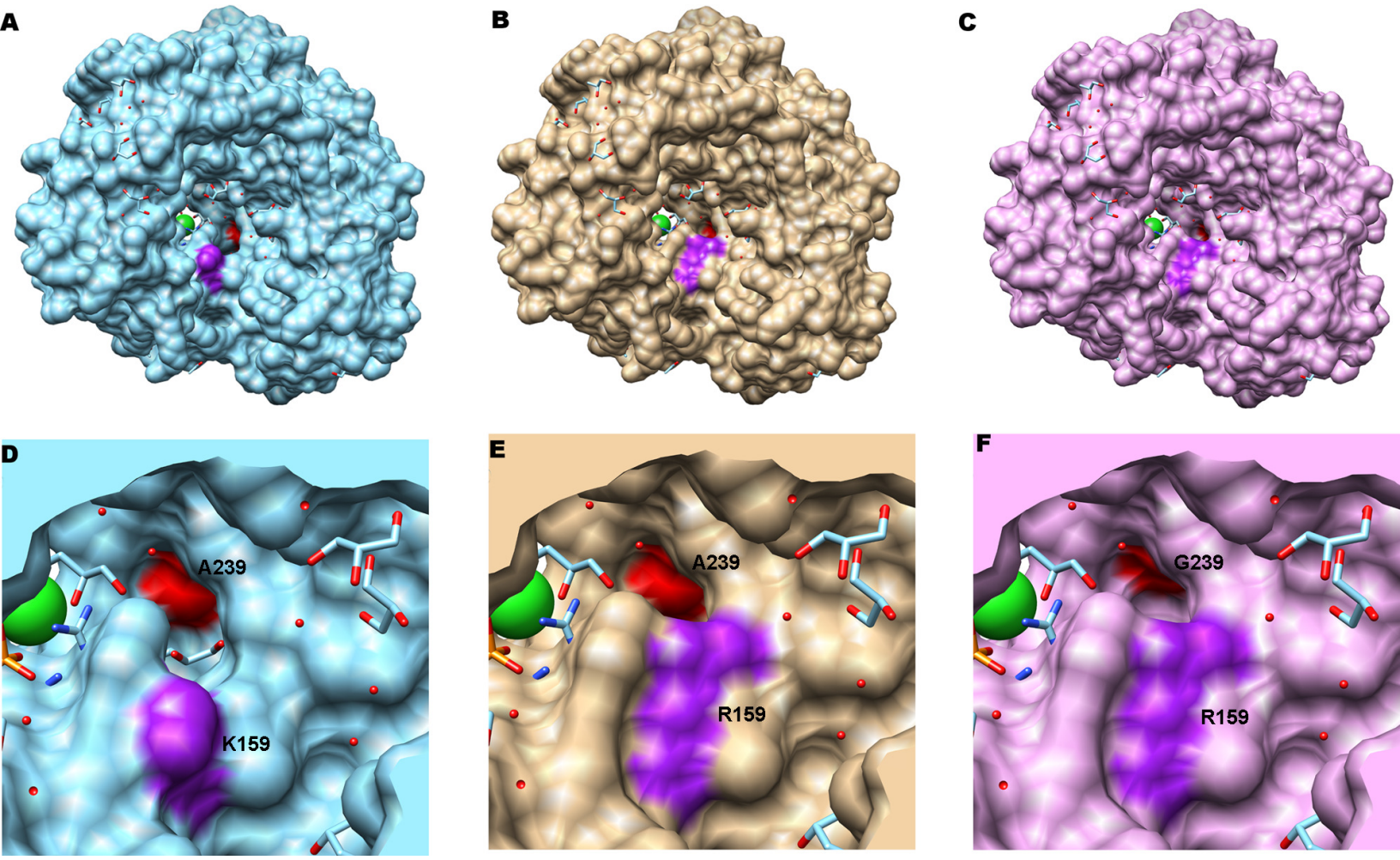
A
B
C
D
A239
K159
E
A239
R159
F
G239
R159

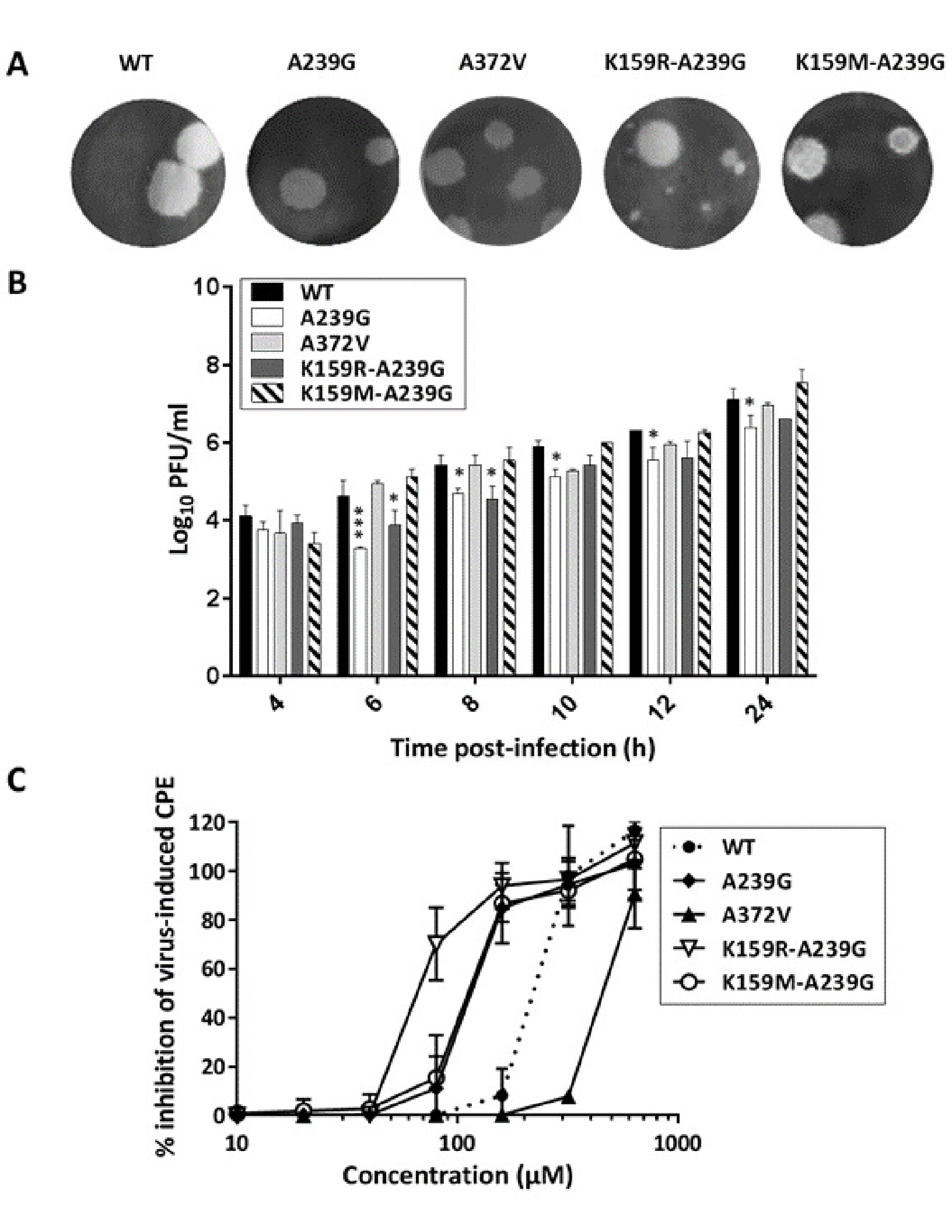
A
WT
A239G
A372V
K159R-A239G
K159M-A239G
B
WT
A239G
A372V
K159R-A239G
K159M-A239G
Log10 PFU/ml
Time post-infection (h)
C
% inhibition of virus-induced CPE
Concentration (μM)
WT
A239G
A372V
K159R-A239G
K159M-A239G

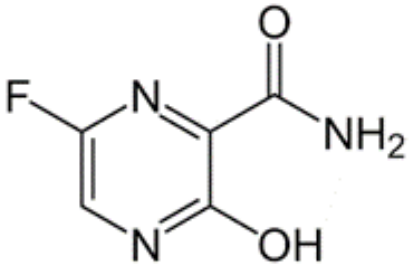

Favipiravir (T-705)

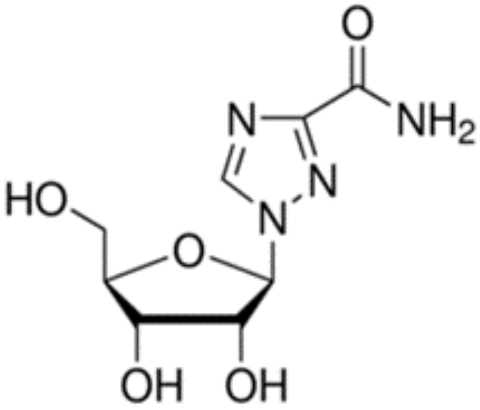

Ribavirin

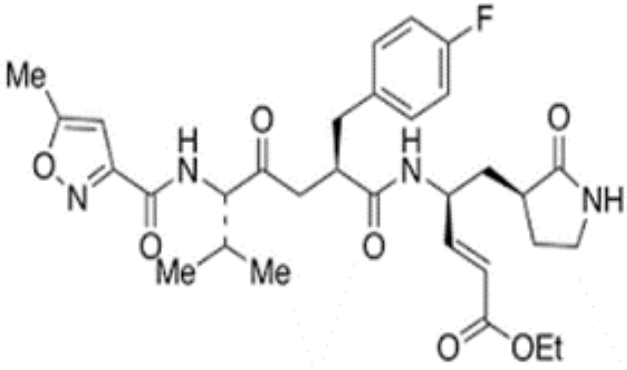

Rupintrivir

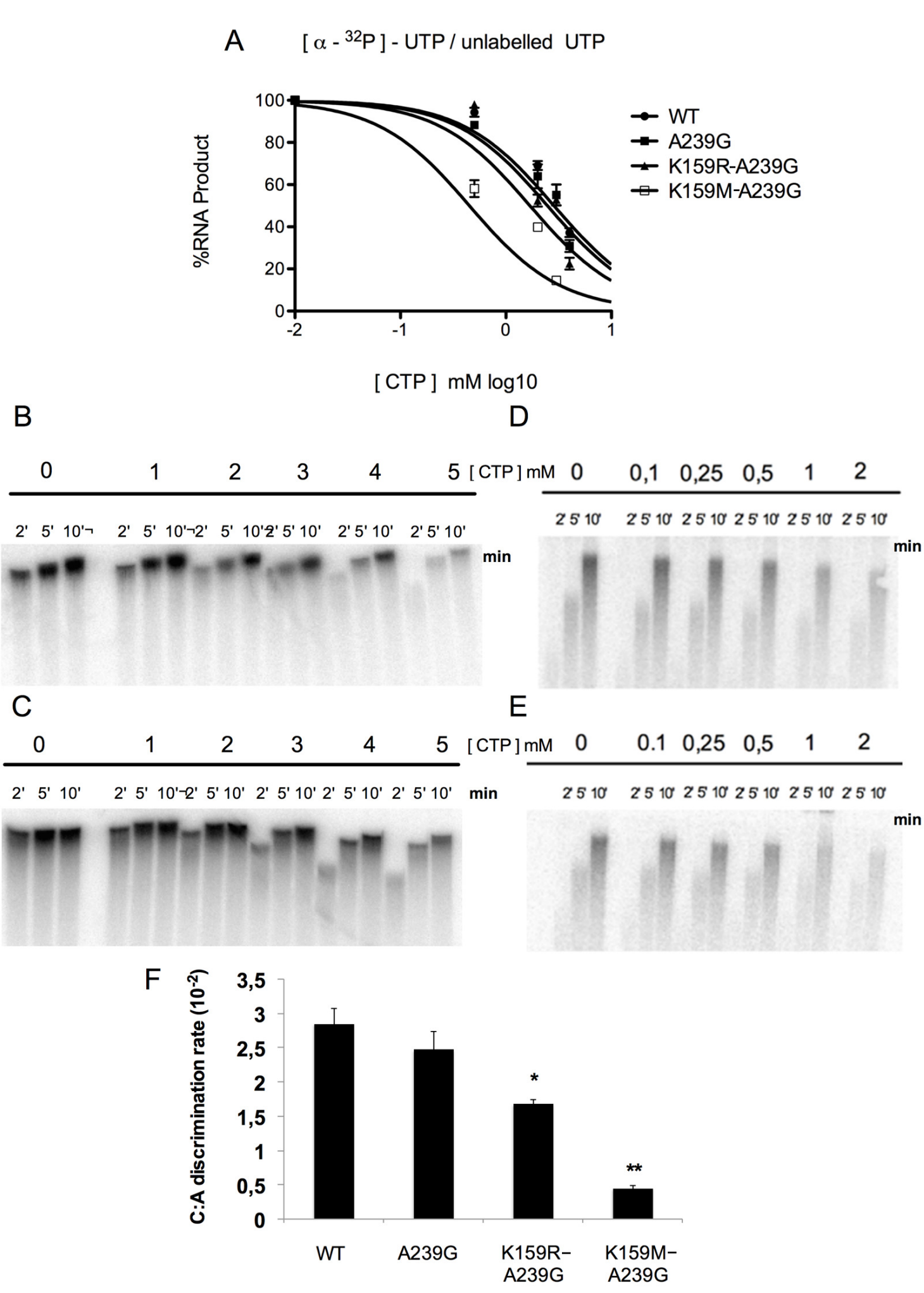
A
[α - 32P] - UTP / unlabelled UTP
%RNA Product
100
80
60
40
20
0
-2
-1
0
1
[CTP] mM log10
WT
A239G
K159R-A239G
K159M-A239G
B
0
1
2
3
4
5
2' 5' 10'
min
D
[CTP] mM 0 0,1 0,25 0,5 1 2
min
C
E
F
C:A discrimination rate (10-2)
3,5
3
2,5
2
1,5
1
0,5
0
*
**
WT
A239G
K159R–A239G
K159M–A239G

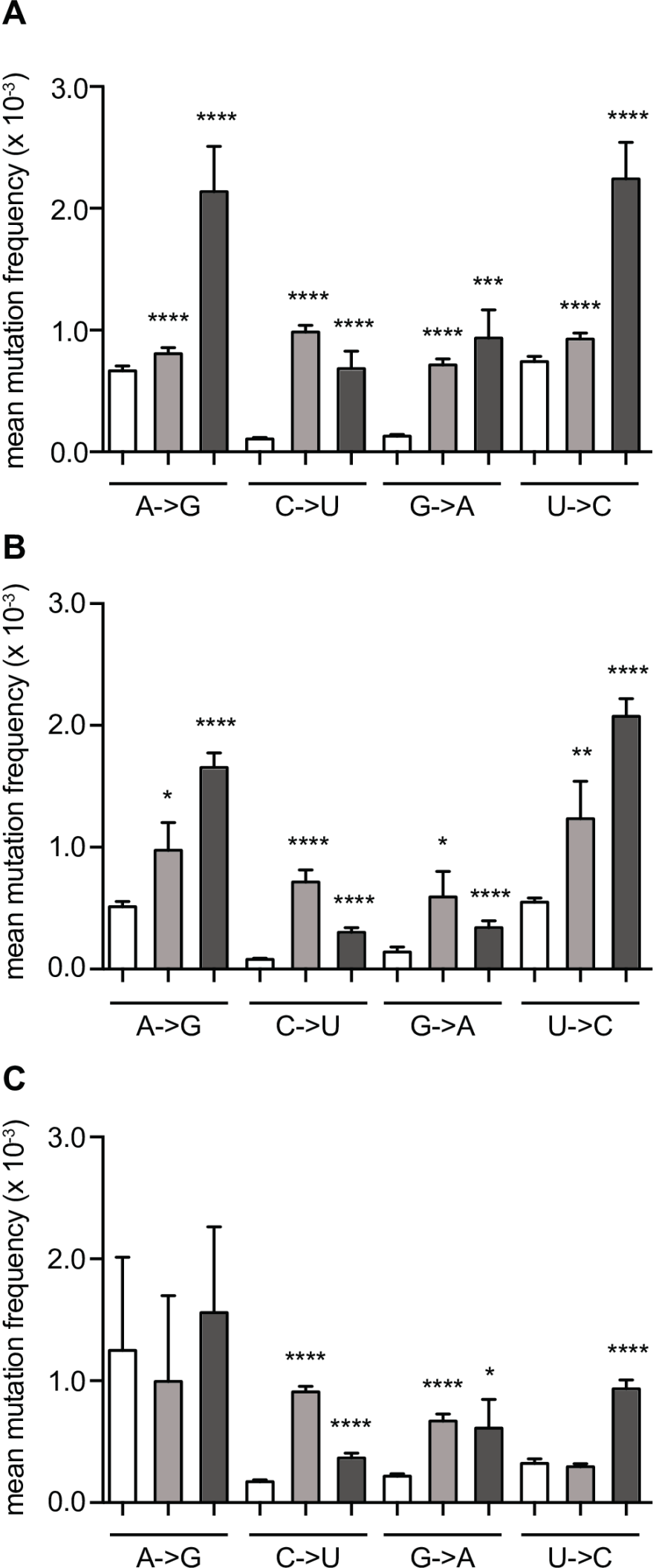
A
mean mutation frequency (x 10-3)
3.0
2.0
1.0
0.0
****
****
****
****
****
***
****
****
A->G
C->U
G->A
U->C
B
mean mutation frequency (x 10-3)
3.0
2.0
1.0
0.0
*
****
****
****
*
****
**
****
A->G
C->U
G->A
U->C
C
mean mutation frequency (x 10-3)
3.0
2.0
1.0
0.0
****
****
****
*
****
A->G
C->U
G->A
U->C

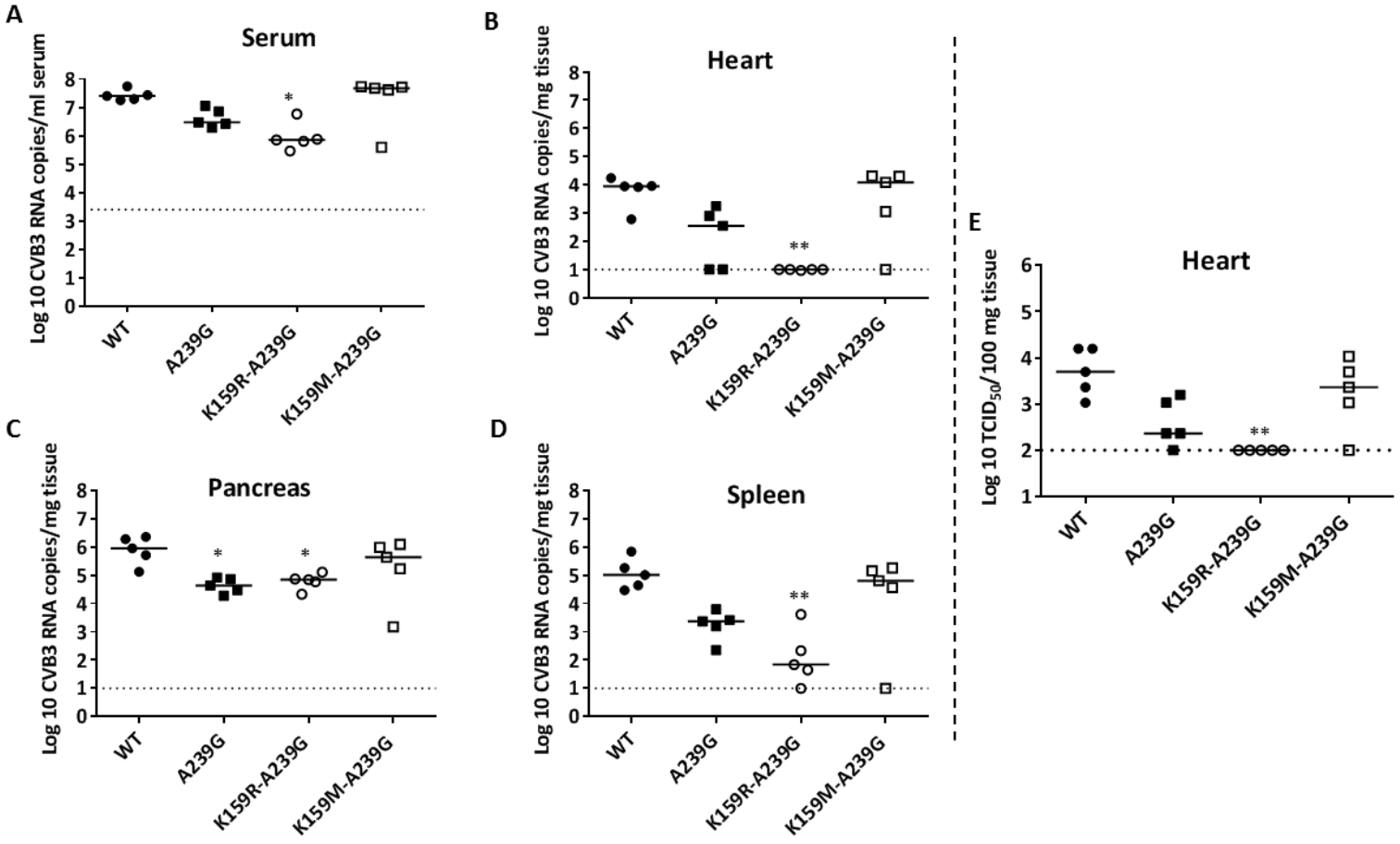
A
Serum
Log 10 CVB3 RNA copies/ml serum
B
Heart
Log 10 CVB3 RNA copies/mg tissue
C
Pancreas
Log 10 CVB3 RNA copies/mg tissue
D
Spleen
Log 10 CVB3 RNA copies/mg tissue
E
Heart
Log 10 TCID50/100 mg tissue
WT
A239G
K159R-A239G
K159M-A239G
*
**